High-temperature laser absorption diagnostics for CH 2 O and CH 3 CHO and their application to shock tube kinetic studies

ARTICLE *in* COMBUSTION AND FLAME · MAY 2013

Impact Factor: 3.08 · DOI: 10.1016/j.combustflame.2013.05.004

3 AUTHORS, INCLUDING:

Shengkai Wang
Stanford University
14 PUBLICATIONS **88** CITATIONS

SEE PROFILE

Combustion and Flame 160 (2013) 1930–1938

Contents lists available at SciVerse ScienceDirect

Combustion and Flame

journal homepage: www.elsevier.com/locate/combustflame

High-temperature laser absorption diagnostics for CH_2O and CH_3CHO and their application to shock tube kinetic studies

Shengkai Wang, David F. Davidson *, Ronald K. Hanson

High Temperature Gasdynamics Laboratory, Mechanical Engineering Department, Stanford University, Stanford, CA, United States

ARTICLE INFO

Article history:
Received 28 February 2013
Received in revised form 3 May 2013
Accepted 3 May 2013
Available online 23 May 2013

Keywords:
Laser absorption
Shock tube
Formaldehyde
Acetaldehyde

ABSTRACT

Laser absorption diagnostic methods were developed for the quantitative measurement of formaldehyde (CH_2O) and acetaldehyde (CH_3CHO) at high temperatures in shock tube kinetic studies. Investigation of the high-temperature CH_2O spectrum has shown that the optimal wavelength for CH_2O detection using commercially available lasers is near 2896 cm^{-1}. By exploiting the structural difference between the absorption spectra of CH_2O and that of broadband interfering species, a two-color (2895.92 cm^{-1} and 2895.60 cm^{-1}) interference-free detection scheme for CH_2O sensing in a combustion environment was developed. A third color (32601.10 cm^{-1}) has also been added to develop a UV/IR detection scheme for combined CH_3CHO/CH_2O measurements. To implement these schemes, aldehyde cross-sections at all three colors were measured behind reflected shock waves over a wide span of temperatures (600–1800 K) and pressures (0.8–3.6 atm), with an uncertainty of ±5%, and the diagnostic schemes were validated using two controlled experiments with well-established chemistry. Applications of these diagnostics were also demonstrated in shock tube pyrolysis experiments of 1,3,5-trioxane, CH_2O and CH_3CHO. The unimolecular decomposition rate of 1,3,5-trioxane was determined over 869–1037 K at an average pressure of 2.1 atm: $k_1 = 3.58 \times 10^{12} \exp(-18{,}590\ K/T)\ s^{-1}$, with an overall uncertainty of less than 20%.

1. Introduction

Aldehydes are important intermediate products in the oxidation of hydrocarbons [1]. They lie on the primary oxidation pathway of alkanes [2,3], form rapidly during the pre-ignition phase of hydrocarbon oxidation [4], and are key species of cool flame reactions [5,6]. Aldehydes are also benchmark species in engine design and testing [7]. They are primary targets of emissions control, and high levels of aldehydes in the exhaust can be a warning of abnormal reaction quenching. In many hydrocarbon combustion processes, the two major aldehydes formed are formaldehyde (CH_2O) and acetaldehyde (CH_3CHO). Accurate quantitative diagnostics for the two species are needed to advance combustion kinetics studies and engine design.

So far, common methods to measure aldehydes in low-temperature kinetic experiments have involved mass spectroscopy (MS) [8] and gas chromatography (GC) [9]. Despite their success in kinetics model development, these methods usually require the reaction to be quenched before sampling and therefore are not suitable for time-resolved *in situ* species history measurements. Laser-induced fluorescence (LIF) has also been demonstrated for time- and space-resolved formaldehyde measurements in engine environments [10–12], but typically requires a calibration experiment with formaldehyde seeding and can suffer from broadband interference emission from hydrocarbons. On the other hand, laser absorption spectroscopy is an *in situ*, time-resolved, and potentially interference-free method for species time history measurement [13], and is a promising technique for aldehyde detection.

There have been several studies of quantitative absorption detection of formaldehyde in shock tubes, using 174 nm UV-absorption [14,15] and 3.39 μm IR-absorption [16,17]. Recent advance in mid-IR lasers [18–20] has enabled access to much stronger transitions of CH_2O near 3.6 μm, and has spurred the development of several novel room temperature sensors for CH_2O [21,22]. While there are multiple candidate wavelengths for formaldehyde detection, this work focuses on finding the best way to measure formaldehyde in high-temperature shock tube kinetics experiments. Using the latest spectroscopic database from Perrin et al. [23] and Jacquemart et al. [24], we have identified, within the capability of current commercially available lasers, the optimal wavelength for CH_2O detection at combustion conditions. A two-color IR CH_2O detection scheme has also been developed, which eliminates broadband interference absorption when it is present. In the case of acetaldehyde, fewer studies have been done using absorption diagnostics. Cook et al. [25] have measured the overall absorption of CH_2O and CH_3CHO during *n*-butanol pyrolysis at 306.8 nm, a few wavenumbers away from the A–X(0,0) $R_1(5)$ OH transition.

* Corresponding author.
E-mail address: dfd@stanford.edu (D.F. Davidson).

0010-2180/$ - see front matter © 2013 The Combustion Institute. Published by Elsevier Inc. All rights reserved.
http://dx.doi.org/10.1016/j.combustflame.2013.05.004

The current work revisits Cook's method and extends the aldehydes cross-section measurement to a wider temperature range. Used in conjunction with the interference-free CH_2O diagnostic, we have also established a three-color combined UV/IR scheme for simultaneous CH_2O and CH_3CHO detection. The method can easily be extended to a four-color aldehydes/OH diagnostic for systems where OH may also be present.

2. Wavelength selection

2.1. IR wavelengths for CH_2O detection

The ultimate goal of wavelength selection is to find a wavelength where (1) the sensitivity of the target species is maximized, and (2) the interfering absorption from other species is minimized. To achieve this goal, quantitative CH_2O absorption spectra in the UV and IR are needed. However, although various studies have been reported on room-temperature CH_2O absorption spectra [26–30], quantitative measurements at high temperatures are quite limited. An estimate of the high-temperature spectra can be obtained through spectroscopic simulations using a line-by-line transition database.

The latest version of the HITRAN database (HITRAN 2008 [31]) fits this purpose well, as it has incorporated the recent updates on CH_2O line intensities from Perrin et al. [23]. In our calculation, the line-broadening coefficients are also updated with the new values from Jacquemart et al. [24]. Absorption spectra of major potential interfering species (H_2O, CO, CO_2 and CH_4) are also calculated using HITRAN 2008.

Figure 1 shows the IR absorption spectra of CH_2O at 296 K and at 1200 K. The whole IR spectrum of CH_2O can be divided into two regions. The 3.6 μm region is the location of the strongest infrared bands of formaldehyde [23], namely the ν_1 (centered around 2782 cm^{-1}) and ν_5 (centered around 2844 cm^{-1}) bands together with several weaker overtones or combination dark bands, and is accessible with difference-frequency-generation (DFG) lasers. The 5.7 μm region is the location of the ν_2 band centered at 1746 cm^{-1}, which is accessible with quantum cascade lasers (QCL).

Although the 5.7 μm region may seem attractive for CH_2O detection due to its stronger peak absorption feature, comparison with potential interferers (Fig. 2) has suggested that this band

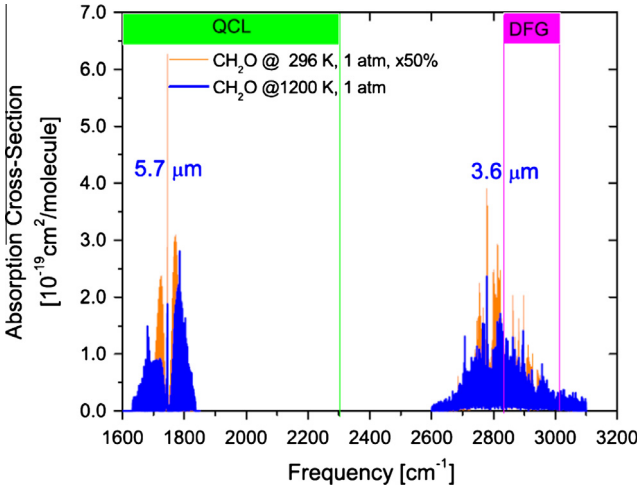

Fig. 1. IR absorption spectra of CH_2O, calculated using data from Perrin et al. [23] and Jaquemart et al. [24]. Blue: 1200 K, 1 atm; gray: 298 K, 1 atm (scaled by 50% for comparison). Also shown are the tuning ranges of lasers that currently are commercially available. (For interpretation of the references to color in this figure legend, the reader is referred to the web version of this article.)

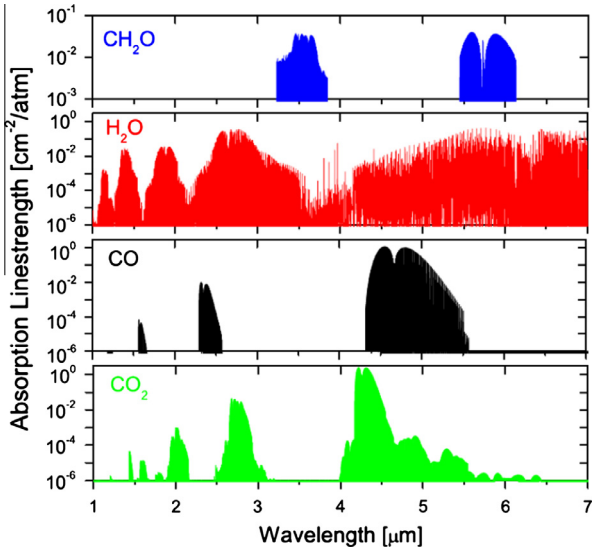

Fig. 2. Absorption line-strengths of CH_2O, H_2O, CO and CO_2 at 1200 K, calculated using HITRAN 2008 [31].

may suffer from strong interference from H_2O, and therefore is not suitable for CH_2O sensing in a combustion environment. On the other hand, the 3.6 μm region is completely free from CO and CO_2 interference, and H_2O interference is, on average, two orders of magnitude weaker. In this region, the strongest transition within laser tuning range of our current laser occurs near 2896 cm^{-1}. Compared to the strongest transition in the whole IR spectrum of CH_2O, this transition is less than 50% weaker, leaving little room for significant improvement on CH_2O sensitivity even when new lasers become available. A closer examination of the CH_2O spectrum (Fig. 3) within 2890–2900 cm^{-1} also indicates that the 2896 cm^{-1} transition is free from H_2O interference.

To eliminate other possible interference absorption, particularly the broadband interference from large hydrocarbon molecules, a two-color differential absorption scheme is proposed. The absorption feature of CH_2O near 2896 cm^{-1} is very narrow (FWHM ≈ 0.3 cm^{-1}), and for most hydrocarbons, their absorption cross-sections are effectively constant across this narrow feature. Therefore by tuning on and off the peak of the CH_2O feature, we can easily subtract the interference absorbance from the total

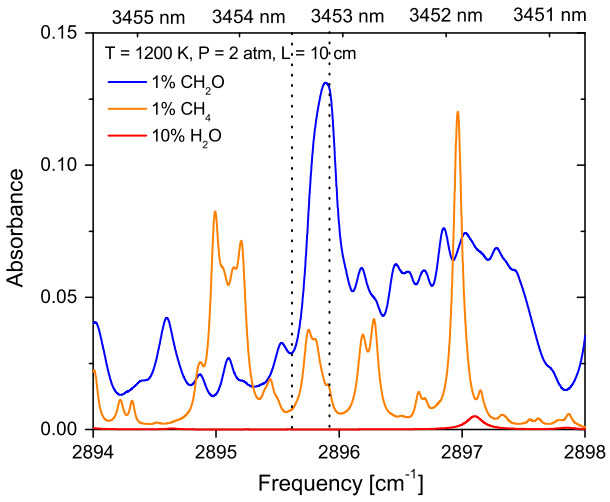

Fig. 3. Absorption spectra of CH_2O, CH_4 and H_2O near 2895 cm^{-1}, calculated using HITRAN 2008 [31]. Dash lines are line pairs from current study.

absorbance to capture only the CH_2O absorbance. A similar two-color absorption scheme has been used for CH_4 detection in heptane chemistry [32], and has proved quite successful for eliminating interference from species with two or more carbon atoms. However, the off-line wavelength cannot be chosen randomly. As an exception to the general broadband character of hydrocarbons, CH_4 also has narrow absorption features (Fig. 3), and was the major constraint on our line pair selection. By trying to (1) maximize the differential absorption cross-section of CH_2O and (2) match the absorption cross-sections and temperature variation of CH_4 at the two wavelengths, we have carefully picked a line pair for CH_2O detection: 2895.92 cm^{-1} (on-line) and 2895.60 cm^{-1} (off-line), which is expected to work over a wide range of temperatures (900–1800 K) and pressure (0.5–5 atm).

To verify our assumptions on the structural differences between the absorption spectra of CH_2O and that of potential interfering species, we have measured their absorption cross-sections as functions of wavelength in a shock tube. Figure 4 shows the shapes of the absorption features of CH_2O and CH_4 near 2896 cm^{-1}. As a representative broadband interfering species, CH_3CHO is also shown on the plot. The flat CH_3CHO spectrum validates our two-color scheme for eliminating broadband interference. Although the interference from CH_4 cannot be completely removed, the differential absorption cross-section of CH_2O is more than 20 times larger than that of CH_4 between the wavelength pair. And because CH_2O typically has a shorter characteristic timescale than CH_4 during hydrocarbon oxidation, this differential sensitivity is often sufficient for successful early-time detection of CH_2O in combustion process, where the concentration of CH_2O can be an order of magnitude higher than that of CH_4.

2.2. UV wavelengths for CH_2O and CH_3CHO detection

Our measurement (Fig. 4) and calculation (Fig. 1) of aldehydes spectra indicates that there is no simple two-color scheme to separate CH_3CHO from broad-band interference in the IR, and therefore CH_3CHO must be measured in another wavelength region such as the UV. Shown in Fig. 5 are the room temperature UV absorption spectra of both aldehydes near 306 nm. As a result of the overlap between the two spectra, a unique determination of the CH_3CHO concentration requires a combined CH_2O/CH_3CHO detection scheme involving both IR and UV lasers. For the UV wavelength selection, the absorption features around 307 nm are attractive, because (1) they lie in the middle of the tuning range of our frequency-doubled ring dye laser used for OH detection, and (2) the CH_3CHO absorption cross-section is much larger than that of CH_2O. In fact, the wavelength dependence of these aldehyde absorption cross-sections is much weaker at high temperatures, and as long as one can avoid OH transitions, a few wavenumbers' change in the wavelength makes little difference (Fig. 6). This lack of variation in absorption cross-section has been confirmed in the previous study of Cook et al. [25]. In the current work, 32601.10 cm^{-1} (306.738 nm) was used as the UV color for aldehydes detection. The detection scheme can be easily extended to include OH detection by the addition of another color at 32606.52 cm^{-1}.

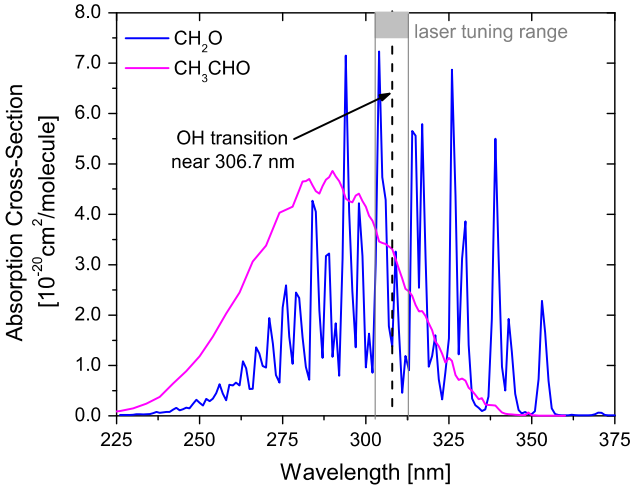

Fig. 5. UV absorption spectra of CH_3CHO and CH_2O at 296 K, 1 atm. Also shown in the plot is the tuning range of our frequency-doubled ring dye laser.

2.3. A quantitative aldehyde detection scheme

The fractional transmission (I/I_0) of a monochromatic light is related to the mole fraction of the absorbing species (χ_i) through the Beer–Lambert relation:

$$-\ln\left(\frac{I}{I_0}\right)_\lambda = \sigma(\lambda,T,P)\chi_i nL = \alpha(\lambda,T,P) \quad (1)$$

where σ is the absorption cross-section of the absorbing species, n is the total number density of the test gas, and L is the path-length.

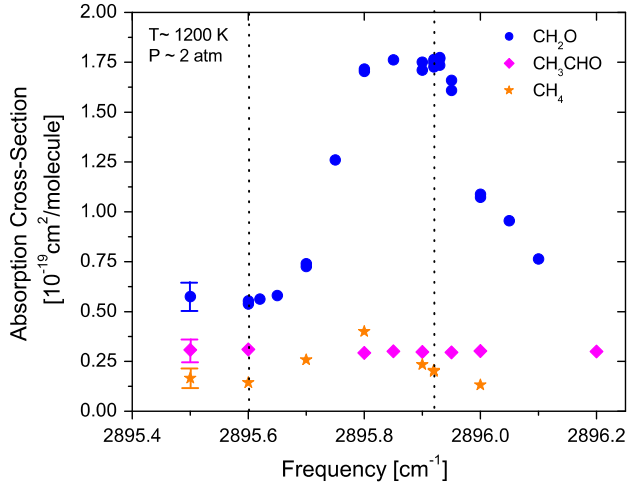

Fig. 4. Measured absorption spectra of CH_2O, CH_3CHO and CH_4 near 2896 cm^{-1}, at 1200 K, 2 atm.

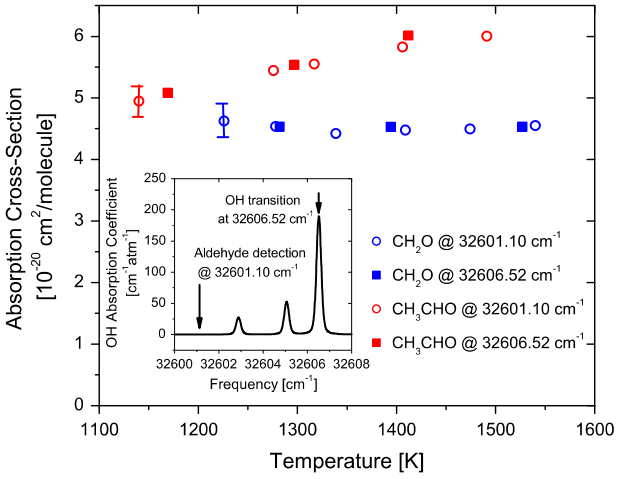

Fig. 6. Wavelength- and temperature-dependence of aldehyde absorption coefficients.

The absorption signal is usually expressed in the form of absorbance (α).

Applying the Beer–Lambert law at the three colors selected for aldehydes detection, namely $\tilde{\nu}_{IR,1} = 2895.92\ \text{cm}^{-1}$, $\tilde{\nu}_{IR,2} = 2895.60\ \text{cm}^{-1}$, $\tilde{\nu}_{UV,1} = 32601.10\ \text{cm}^{-1}$, together with the OH color at $\tilde{\nu}_{UV,2} = 32606.52\ \text{cm}^{-1}$, we have a closed set of equations with an equal number of unknowns (χ_{CH_2O}, χ_{CH_3CHO}, χ_{OH}, and the interference absorbance α_{int}):

$$\alpha_{IR1} = \alpha_{CH_2O,IR1} + \alpha_{int} = \sigma_{CH_2O,IR1}\chi_{CH_2O}nL + \alpha_{int} \quad (2)$$

$$\alpha_{IR2} = \alpha_{CH_2O,IR2} + \alpha_{int} = \sigma_{CH_2O,IR2}\chi_{CH_2O}nL + \alpha_{int} \quad (3)$$

$$\alpha_{UV1} = \alpha_{ald,UV} = (\sigma_{CH_2O,UV}\chi_{CH_2O} + \sigma_{CH_3CHO,UV}\chi_{CH_3CHO})nL \quad (4)$$

$$\alpha_{UV2} = \alpha_{ald,UV} + \alpha_{OH} = (\sigma_{CH_2O,UV}\chi_{CH_2O} + \sigma_{CH_3CHO,UV}\chi_{CH_3CHO} + \sigma_{CH_2O,UV}\chi_{CH_2O} + \sigma_{OH}\chi_{OH})nL \quad (5)$$

Given the knowledge of their absorption cross-sections we can solve for the mole fractions of aldehydes and OH. Particularly, from the two-color CH_2O scheme ((2) and (3)),

$$\chi_{CH_2O} = \frac{\alpha_{IR1} - \alpha_{IR2}}{(\sigma_{CH_2O,IR1} - \sigma_{CH_2O,IR2})nL} \quad (6)$$

The three-color aldehydes scheme (2)–(4) yields

$$\chi_{CH_3CHO} = \left[\alpha_{UV1} - \frac{\sigma_{CH_2O,UV}(\alpha_{IR1} - \alpha_{IR2})}{\sigma_{CH_2O,IR1} - \sigma_{CH_2O,IR2}}\right] \Big/ \sigma_{CH_3CHO,UV}nL \quad (7)$$

And the OH mole fraction, when of interest, is given by

$$\chi_{OH} = \frac{\alpha_{UV2} - \alpha_{UV1}}{\sigma_{OH}nL} \quad (8)$$

3. Absorption cross-section measurement

Absorption cross-sections of CH_2O were measured behind reflected shock waves using 1,3,5-trioxane as a CH_2O precursor. The experimental setup is shown in Fig. 7. Experiments were carried out in a 14 cm diameter high-purity shock tube. A detailed description of the Stanford shock tube facility can be found in [33]. The two IR wavelengths were probed using a prototype DFG laser from Novawave. The laser has a fixed-wavelength (1064 nm) pump laser, which was mixed with a tunable fiber-coupled DFB laser (centered around 1538 nm) in a temperature-controlled periodically poled lithium niobate (PPLN) crystal for difference-frequency-generation. Similar setups have been explored by Ritcher et al. [34] and Pyun et al. [32]. The PPLN crystal is phase-matched for maximum output in the mid-IR, and a typical output power of 170 μW can be achieved. The IR signals were measured using a liquid-nitrogen-cooled InSb detector with a matched amplifier. The wavelength of the laser was monitored using a Bristol 721 wavemeter, which has a spectral resolution of 0.002 cm^{-1}. The output of the DFG laser was very stable, and over 30 min, its wavelength and power drifts were measured to be less than 0.02 cm^{-1} and 1%, respectively. Two irises and a narrow bandpass spectral filter (Spectragon, center wavelength = 3465 nm, FWHM = 43 nm) were used to minimize the thermal emission from the shock-heated gas mixture. Minimum IR detection of 0.3% absorption could be achieved over the test time (2 ms) of shock tube experiments. The 306.7 nm UV light was generated using intracavity frequency-doubling with a temperature-tuned AD * A crystal, from the 613.4 nm visible output of a Spectra Physics 380A ring dye laser. The wavelength of the laser was measured with a Burleigh WA-1000 wavemeter, and the mode quality of the visible light was examined by a scanning interferometer. The laser output was monitored with a pair of Thorlab PDA36A Si amplified detectors, which were shielded with Newport FSR-UG11 filters to reduce broadband interference emission. Common mode rejection was used to reduce the noise of measurements to less than 0.3%.

High-purity trioxane (>99%) and acetaldehyde (>99.5%), supplied by Sigma–Aldrich, were purified using a freeze-pump-thaw method to remove dissolved air. Research grade high-purity gases (argon and helium; >99.999%), supplied by Praxair, Inc. (San Ramon, CA), were used without further purification. Gas mixtures of 0.333%, 0.167% and 0.083% trioxane/Ar (equivalent to

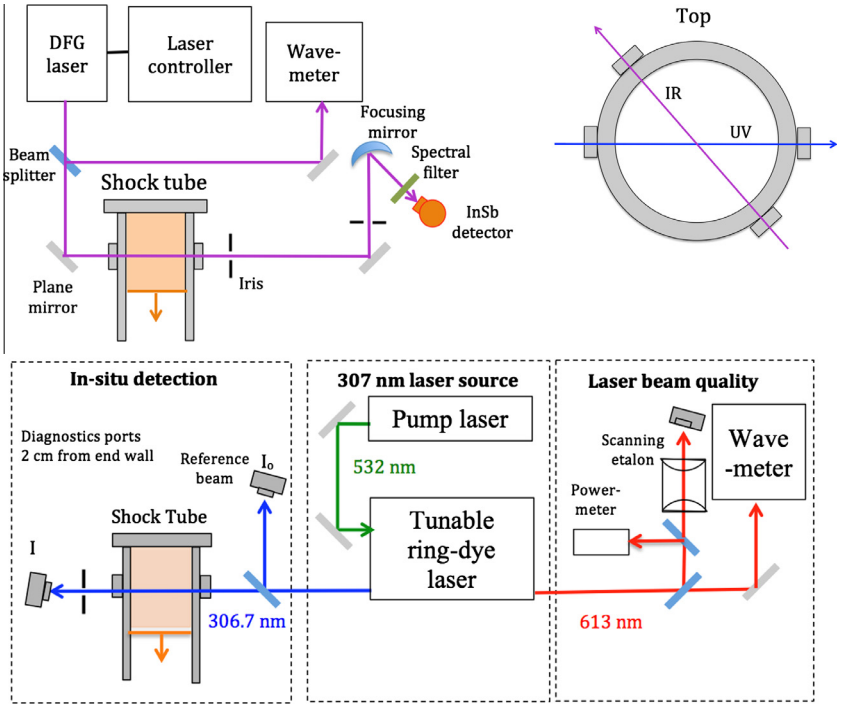

Fig. 7. Experimental setup (top: IR; bottom: UV).

1%, 0.5% and 0.25% CH_2O/Ar, respectively) were filled into the driven section of the shock tube to the desired initial pressures. Depending on the temperatures behind the reflected shock waves, three distinct types of absorption signal have been observed (Fig. 8). At low temperatures (870–1050 K), we were able to observe the decomposition of trioxane and use the plateau absorbance to determine CH_2O cross-sections. In the temperature range of 1050–1400 K, after trioxane decomposes near-instantaneously into CH_2O, highly uniform absorption profiles were obtained. At even higher temperatures, CH_2O began to fall apart within our test time, and its absorption cross-sections were determined immediately after the arrival of the reflected shock wave. Extrapolation of the absorption signal was needed for very high temperatures (>1700 K). Similar experiments have been done on 1%, 0.5% and 0.25% CH_3CHO/Ar mixtures, and the CH_3CHO absorption cross-sections were measured behind both incident and reflected shock waves, over a wide span of temperature ($592\ K < T_2 < 955\ K$, $918\ K < T_5 < 1672\ K$).

Figure 9 shows measured IR absorption cross-sections of CH_2O. The uncertainty in the absorption coefficient obtained through these experiments, estimated to be ±5%, was the result of uncertainties in experimental temperature and pressure and uncertainties in the concentration of CH_2O precursors. The CH_2O absorption cross-sections at the two IR wavelengths were fitted (Fig. 10) as functions of temperature and pressure. The least-squares fits yield:

$$\sigma_{CH_2O,2895.92\ cm^{-1}}\ [cm^2/molecule] = 1.346 \times 10^{-7} T[K]^{-3.564} \exp(-2277/T[K]) P[atm]^{-0.283}$$

$$\sigma_{CH_2O,2895.60\ cm^{-1}}\ [cm^2/molecule] = 4.904 \times 10^{-17} T[K]^{-0.961} \exp(-165.6/T[K]) P[atm]^{0.256}$$

These expressions are valid over 900–1800 K and 0.8–3.3 atm, conditions at which the HITRAN 2008 model has yet to be optimized.

Figure 11 shows the measured UV absorption cross-sections of CH_3CHO and CH_2O. No pressure dependence was observed for either species. The least-square fits

$$\sigma_{CH_2O,32601.10\ cm^{-1}}\ [cm^2/molecule] = 4.578 \times 10^{-20}$$

$$\sigma_{CH_3CHO,32601.10\ cm^{-1}}\ [cm^2/molecule] = 9.022 \times 10^{-21} + 4.225 \times 10^{-23} T - 2.096 \times 10^{-26} T[K]^2$$

are valid over the ranges 900–1600 K and 500–1700 K, respectively, and are seen to agree with the measurement within an RMS error of 3%.

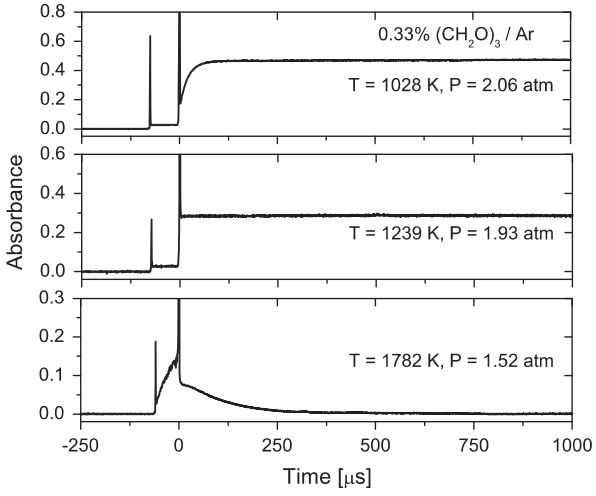

Fig. 8. Sample CH_2O absorbance traces.

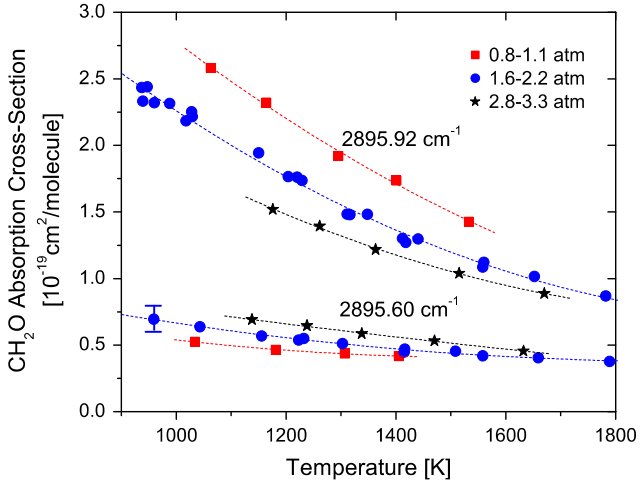

Fig. 9. Temperature dependence of CH_2O IR cross-sections at three pressures. Dash lines are best fit for each pressure.

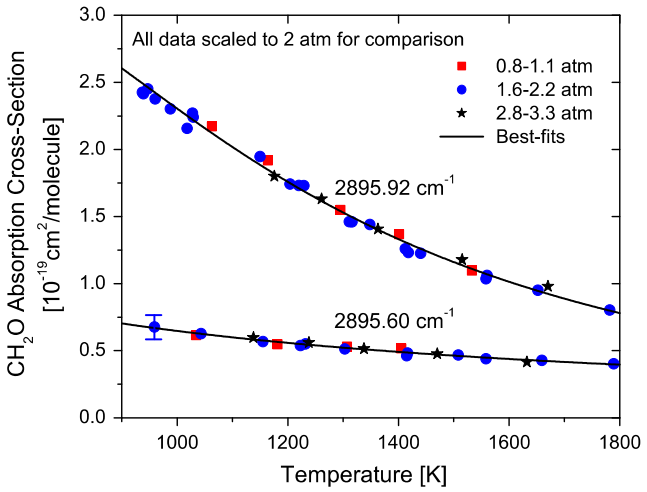

Fig. 10. Fitted IR absorption cross-sections of CH_2O.

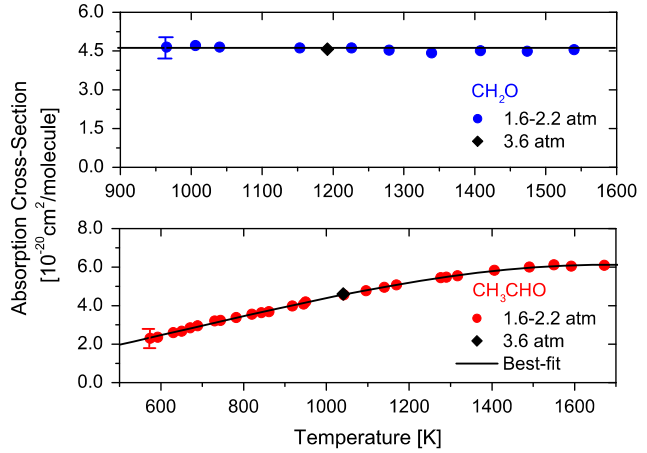

Fig. 11. UV absorption cross-sections of CH_2O and CH_3CHO at 32601.10 cm^{-1}.

4. Validation experiments

The performance of the 4-color $CH_2O/CH_3CHO/OH$ diagnostic scheme has been validated through two controlled experiments, where mixture of 0.167% trioxane/0.5% CH_3CHO/Ar were pyrolyzed behind reflected shock waves. The first experiment was performed at a low temperature where we could observe the formation of CH_2O through trioxane pyrolysis. Figure 12 shows example measured absorbances at the four wavelengths. Figure 13 shows that we have completely separated the absorption signals of CH_2O and CH_3CHO, and successfully recovered the expected values of their steady-state concentrations. The second experiment was conducted at a high temperature where the aldehydes could rapidly fall apart. Figure 14 shows that we have recovered the initial aldehyde concentrations and captured their long-time trend of decay. Both aldehyde concentrations decay to zero as time increases, and their decay rates are similar, suggesting that they may be coupled through reactions with intermediate radical species, which agrees well with chemical kinetic simulations. As expected, no OH was detected in either experiment.

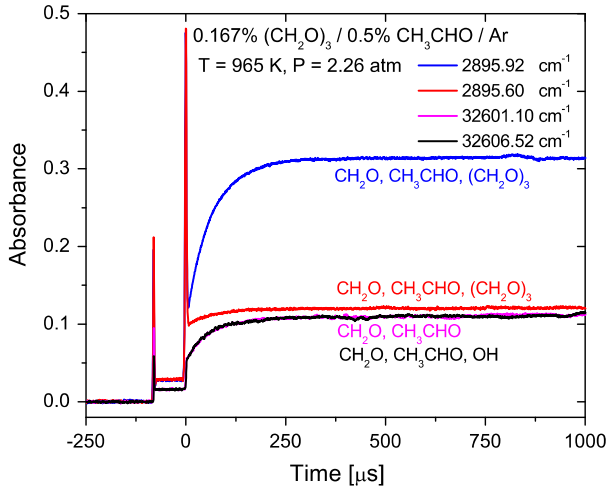

Fig. 12. Four-color absorption time history of 0.167% trioxane/0.5% CH_3CHO/Ar mixture with initial reflected shock conditions of 965 K and 2.26 atm. The 32601.10 cm^{-1} and 32606.52 cm^{-1} data are almost coincident, as expected. (For interpretation of the references to color in this figure legend, the reader is referred to the web version of this article.)

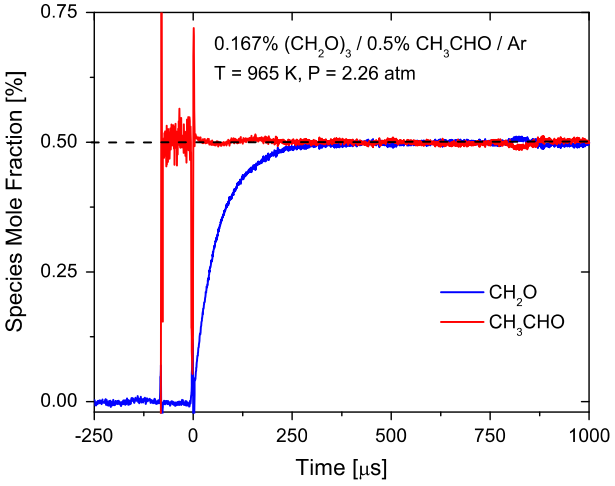

Fig. 13. Measured aldehydes time histories of 0.167% trioxane/0.5% CH_3CHO/Ar for initial reflected shock conditions of 965 K and 2.26 atm.

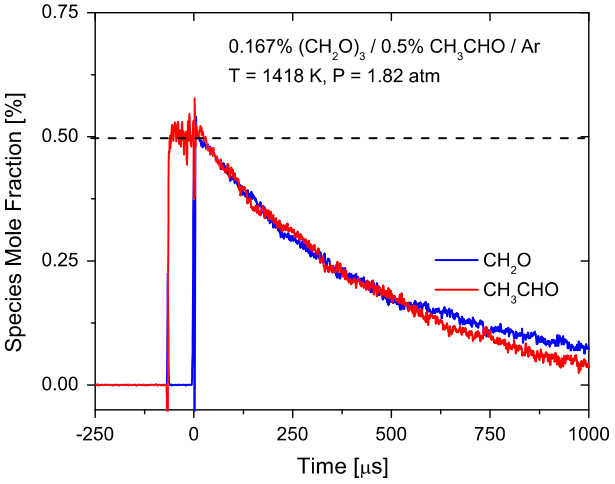

Fig. 14. Measured aldehydes time histories of 0.167% trioxane/0.5% CH_3CHO/Ar for initial reflected shock conditions of 1418 K and 1.82 atm.

5. Example applications

5.1. Trioxane pyrolysis

The new CH_2O diagnostics have allowed direct measurements of the rate coefficient for the unimolecular decomposition of 1,3,5-trioxane in reflected shock wave experiments:

$$1,3,5\text{-trioxane} \rightarrow CH_2O + CH_2O + CH_2O \qquad (I)$$

Within the temperature range of 800–1100 K, CH_2O is the only product from trioxane decomposition, and the mole fraction of trioxane is directly related to CH_2O through carbon balance. Since in this situation interference absorption was not an issue, a single-wavelength detection method for CH_2O was used to achieve higher accuracy. Both the UV wavelength (32601.10 cm^{-1}) and the IR wavelength (2896.92 cm^{-1}) were used in these experiments, and yielded consistent results. As the decomposition of trioxane is dominated by only one reaction (I), the exponential time constant is directly related to the rate coefficient k_I. The decomposition rates k_I have been determined by fitting the CH_2O time history (Fig. 15) to an exponential form of $Cexp(-k_I t)$. Results of the rate measurements are listed in Table 1.

Over the temperature range (869–1037 K) of this measurement, the decomposition rate was fit to an Arrhenius form:

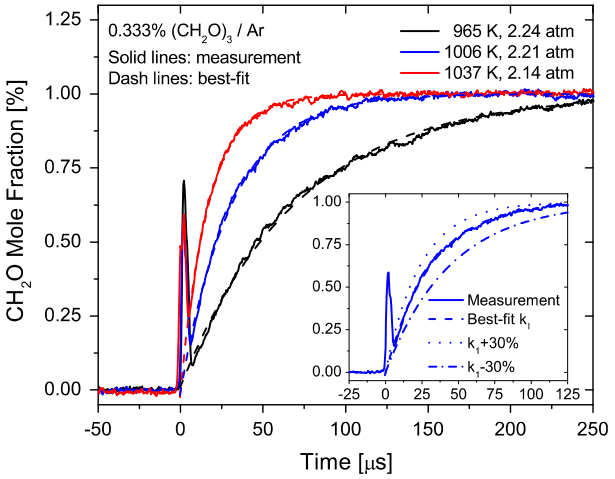

Fig. 15. Sample CH_2O traces during trioxane decomposition.

Table 1
Measured unimolecular decomposition rate of 1,3,5-trioxane.

Temperature (K)	Pressure (atm)	k_I (1/s)
869[a]	2.04	1.90×10^3
889[a]	2.05	2.62×10^3
935[a]	1.99	8.55×10^3
939[b]	2.27	9.80×10^3
947[a]	2.03	1.10×10^4
965[c]	2.24	1.41×10^4
967[b]	2.18	1.66×10^4
988[a]	1.97	2.55×10^4
1006[c]	2.21	3.20×10^4
1025[a]	2.06	4.73×10^4
1029[a]	2.08	5.18×10^4
1033[a]	2.08	5.39×10^4
1036[a]	2.14	5.75×10^4
1037[c]	2.14	5.80×10^4

[a] 0.167% trioxane/Ar.
[b] 0.083% trioxane/Ar.
[c] 0.333% trioxane/Ar.

$$k_I(2.1atm) = 3.58 \times 10^{12}\exp(-18,590\ \mathrm{K/T})\ \mathrm{s}^{-1}$$

with RMS error less than 5%. The overall uncertainty in k_I was estimated to be less than 20%, which derives from uncertainties in temperature behind the reflected shock wave (1%) and in exponential fitting of the absorption profile (10%).

Figure 16 compares current results with previous shock tube measurements from Irdam and Kiefer [35] using laser Schlieren, and flow-reactor measurements from Hochgreb and Dryer [36] using gas chromatography. Our data agree very well with Irdam et al., and has extended the experimental conditions closer to the high-pressure limit. However, due to the uncertainty in their falloff parameters, Irdam's values of k_∞, calculated from RRKM extrapolation, are larger than found in the current study by a factor of 4. Our new data also bridge the temperature gap between Irdam's and Hochgreb's experiments.

5.2. CH_2O pyrolysis

As another example application, CH_2O pyrolysis time histories have been measured behind reflected shock waves from 1560 to 1782 K, using laser absorption at 2895.92 cm^{-1}. Figure 17 shows three representative traces. The current measurements allowed validation of reaction mechanisms developed for CH_2O chemistry. As an example, the performance of USC-Mech II [37], a small mechanism optimized for the high-temperature chemistry of H_2, CO and C_1–C_4 compounds, has been analyzed. Excellent agreement is seen for the case of 1560 K. However, at higher temperatures, the simulations using the USC-Mech II mechanism underpredict the decay rates of CH_2O by 20–40%. Local sensitivity analysis (Fig. 18) has revealed that the CH_2O concentration in these experiments was most sensitive to the following reactions:

$$HCO + H(+M) = CH_2O(+M) \quad \text{(II)}$$

$$CH_2O + H = HCO + H_2 \quad \text{(III)}$$

$$HCO + M = H + CO + M \quad \text{(IV)}$$

$$HCO + H = CO + H_2 \quad \text{(V)}$$

Studies from Friedrichs et al. [38] have provided more accurate expressions for the reaction rate coefficient k_{II}, valid for 1400–3000 K. After we update the USC-Mech II with the more recent values of k_{II}, much better agreement with high-temperature experiments was obtained (Fig. 17).

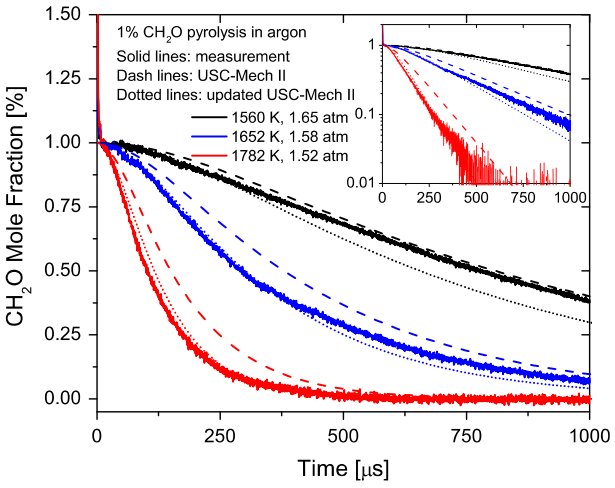

Fig. 17. Comparison of measured and simulated CH_2O traces for 0.33% trioxane (equivalent to 1% CH_2O)/Ar. Simulations used USC Mech II [37].

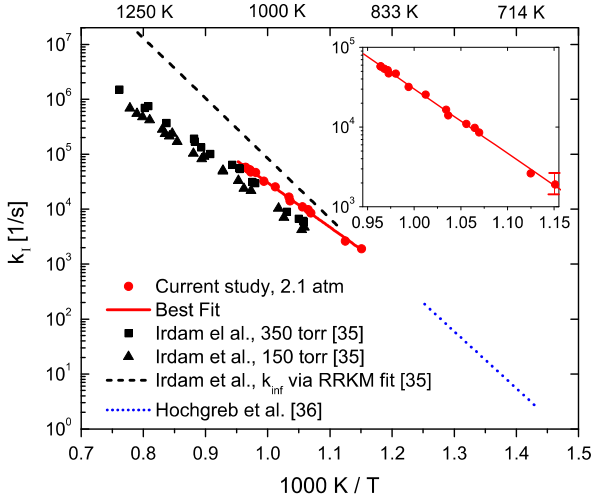

Fig. 16. Comparison of measured k_I with previous studies.

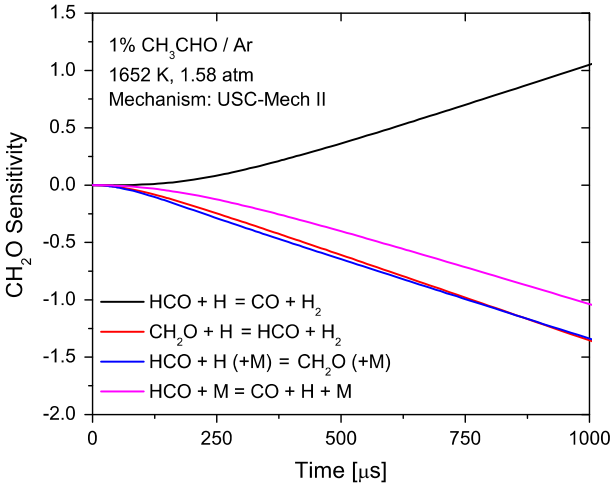

Fig. 18. Sensitivity analysis of 1% CH_2O pyrolysis in Ar using USC Mech II [37].

5.3. CH_3CHO pyrolysis

The thermal decomposition of CH_3CHO has been measured behind reflected shock waves using UV absorption at 32601.10 cm^{-1} and compared with kinetic simulation (Fig. 19). Again, simulations using the USC-Mech II mechanism underpredict the decay rates of CH_3CHO. Sensitivity analysis (Fig. 20) suggests that the following reactions are responsible for this:

$$CH_3 + HCO(+M) = CH_3CHO(+M) \quad (VI)$$

$$CH_3CHO + CH_3 = CH_3CO + CH_4 \quad (VII)$$

$$CH_3 + CH_3(+M) = C_2H_6(+M) \quad (VIII)$$

$$CH_3CHO + H = CH_3CO + H_2 \quad (IX)$$

Comparisons using an updated USC-Mech II mechanism with revised values for k_{VI} and k_{IX} from Bentz et al. [39] show that while there is some improvement, the updated mechanism still does accurately match our data. Further shock tube/laser absorption species time-histories measurements of other CH_3CHO decomposition products (such as CO, CH_3 and CH_4) should provide kinetics modeling targets that will better constrain the mechanism and allow refinements in key reaction rates.

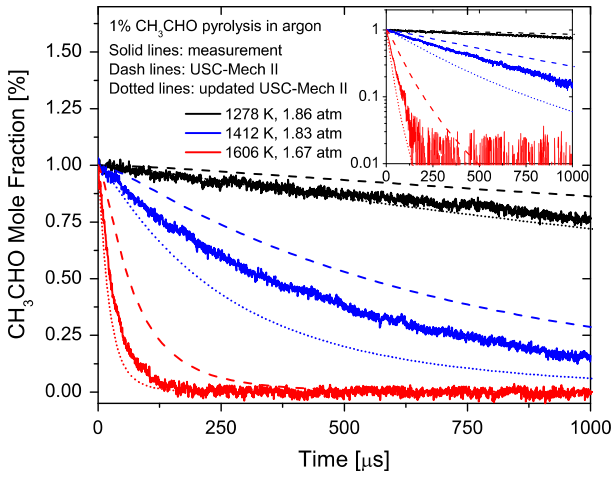

Fig. 19. Comparison of measured and simulated CH_3CHO traces for 1% CH_3CHO/Ar. Simulations used USC Mech II [37].

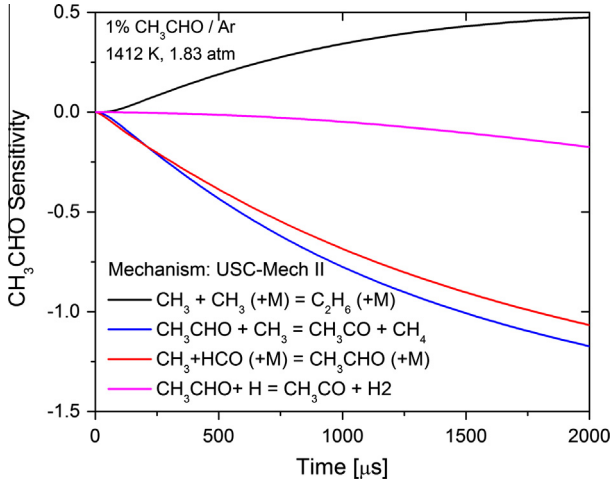

Fig. 20. Sensitivity analysis of 1% CH_3CHO pyrolysis in Ar using USC Mech II [37].

6. Conclusions

A quantitative multi-color laser absorption diagnostics has been developed and validated for optimal CH_2O sensing and combined CH_3CHO/CH_2O detection. The system utilized a tunable DFG laser at 2895.92 cm^{-1} and 2895.60 cm^{-1}, and a frequency-doubled ring dye laser at 32601.10 cm^{-1}. The absorption cross-sections of CH_2O at the two IR wavelengths have been measured behind reflected shock waves over 900–1800 K, 0.8–3.3 atm, with an uncertainty of ±5%. Absorption cross-sections of both aldehydes at the UV wavelength have been measured to the same accuracy, over 900–1600 K and 500–1700 K, respectively.

The diagnostic was then applied to shock tube pyrolysis experiments of 1,3,5-trioxane, CH_2O and CH_3CHO. The unimolecular decomposition rate of 1,3,5-trioxane was determined over 869–1037 K with an overall uncertainty of ±20%. The measured aldehydes decomposition time histories have been compared to kinetic simulations using the USC-Mech II mechanism, which generally underpredicts the decay rates of both aldehydes. Significant improvements in the simulations have been achieved by updating the rate coefficients of one key reaction in the CH_2O pyrolysis mechanism. Improvement in the CH_3CHO chemistry, however, requires further study. Aside from the example applications demonstrated, these diagnostics have great potential for studying other reaction systems, such as the oxidation chemistry of hydrocarbons and pyrolysis of oxygenated fuels. Future shock tube experiments are planned to apply these diagnostics scheme to pyrolysis and oxidation of alcohols, ethers and biodiesel fuel surrogates.

Acknowledgments

This work was supported by the Department of Energy, Office of Basic Energy Sciences, Grant No. DE-FG02-88ER13857, with Wade Sisk, Ph.D. as contract monitor.

References

[1] K.C. Salooja, Combust. Flame 9 (4) (1965) 373–382.
[2] J. Warnatz, in: W.C. Gardiner Jr. (Eds.), Combustion Chemistry, Springer-Verlag, New York, 1984.
[3] G.P. Smith, D.M. Golden, M. Frenklach, N.W. Moriarty, B. Eiteneer, M. Goldenberg, C.T. Bowman, R. Hanson, S. Song, W.C. Gardiner Jr., V. Lissianski, Z. Qin, GRI-Mech Version 3.0, 1999, <http://www.me.berkeley.edu/gri_mech/>.
[4] R.T. Pollard, in: C.H. Bamford, C.F.H. Tipper, (Eds.), Comprehensive Chemical Kinetics, vol. 17, Elsevier, New York, 1977, pp. 249–367.
[5] R.S. Sheinson, F.W. Williams, Combust. Flame 21 (1973) 221–230.
[6] M.P. Halstead, A. Prothero, C.P. Quinn, Combust. Flame 20 (2) (1973) 211–221.
[7] T. Wagner, M.L. Wyszyński, Proceedings of the Institution of Mechanical Engineers, Part D: Journal of Automobile Engineering 210 (2) (1996) 109–122.
[8] J.N. Bradley, G.A. Jones, G. Kirrow, C.F.H. Tippe, Symp. (Int.) Combust. 10 (1) (1965) 139–144.
[9] H. Nishikawa, T. Sakai, J. Chromatogr., A 710 (1) (1995) 159–165.
[10] J.E. Harrington, K.C. Smyth, Chem. Phys. Lett. 202 (3) (1993) 196–202.
[11] A.J. Donkerbroek, A.P. van Vliet, L.M.T. Somers, P.J.M. Frijters, R.J.H. Klein-Douwel, N.J. Dam, W.L. Meerts, J.J. ter Meulen, Combust. Flame 157 (1) (2010) 155–166.
[12] C. Brackmann, J. Nygren, X. Bai, Z. Li, H. Bladh, B. Axelsson, I. Denbratt, L. Koopmans, P.E. Bengtsson, M. Aldén, Spectrochim. Acta, Part A: Mol. Biomol. Spectrosc. 59 (14) (2003) 3347–3356.
[13] R.K. Hanson, P.A. Kuntz, C.H. Kruger, Appl. Opt. 16 (1977) 2045–2048.
[14] H.G. Schecker, W. Jost, Ber. Bunsenges Phys. Chem. 73 (1969) 521–526.
[15] V. Vasudevan, D.F. Davidson, R.K. Hanson, Int. J. Chem. Kinet. 37 (2) (2004) 98–109.
[16] Y. Hidaka, T. Taniguchi, T. Kamesawa, H. Masaoka, K. Inami, H. Kawano, Int. J. Chem. Kinet. 25 (1993) 305–322.
[17] J. Kline, S. Penner, Proc. Int. Symp. Shock Tubes Waves 13 (1982) 869–877.
[18] A. Bauer, M. Dallner, M. Kamp, S. Höfling, L. Worschech, A. Forchel, Opt. Eng. 49 (11) (2010) 111–117.
[19] M. Kim, W.W. Bewley, J.R. Lindle, C.S. Kim, C.L. Canedy, J. Abell, I. Vurgaftman, J.R. Meyer, Laser Applications to Chemical, Security and Environmental Analysis, Optical Society of America, 2010.
[20] L. Naehle, S. Belahsene, M. von Edlinger, M. Fischer, G. Boissier, P. Grech, G. Narcy, A. Vicet, Y. Rouillard, J. Koeth, L. Worschech, Electron. Lett. 47 (1) (2011) 46–47.

[21] D.G. Lancaster, A. Fried, B. Wert, B. Henry, F.K. Tittel, Appl. Opt. 39 (24) (2000) 4436–4443.
[22] S. Lundqvist, P. Kluczynski, R. Weih, M. von Edlinger, L. Nähle, M. Fischer, A. Bauer, S. Höfling, J. Koeth, Appl. Opt. 51 (25) (2012) 6009–6013.
[23] A. Perrin, D. Jacquemart, F. Kwabia Tchana, N. Lacome, J. Quant. Spectrosc. Radiat. Transfer 110 (9) (2009) 700–716.
[24] D. Jacquemart, A. Laraia, F. Kwabia Tchana, R.R. Gamache, A. Perrin, N. Lacome, J. Quant. Spectrosc. Radiat. Transfer 111 (9) (2010) 1209–1222.
[25] R.D. Cook, D.F. Davidson, R.K. Hanson, Int. J. Chem. Kinet. 44 (5) (2012) 303–311.
[26] D.J. Clouthier, D.A. Ramsay, Annu. Rev. Phys. Chem. 34 (1) (1983) 31–58.
[27] F.D. Pope, C.A. Smith, M.N.R. Ashfold, A.J. Orr-Ewing, Phys. Chem. Chem. Phys. 7 (2005) 79–84.
[28] C.A. Smith, F.D. Pope, B. Cronin, C.B. Parkes, A.J. Orr-Ewing, J. Phys. Chem. A110 (2006) 11645–11653.
[29] S.W. Sharpe, T.J. Johnson, R.L. Sams, P.M. Chu, G.C. Rhoderick, P.A. Johnson, Appl. Spectrosc. 58 (2004) 452–1461.
[30] V. Catoire, F. Bernard, Y. Mébarki, A. Mellouki, G. Eyglunent, V. Daële, C. Robert, J. Environ. Sci. 24 (1) (2012) 22–33.
[31] L.S. Rothman, I.E. Gordon, A. Barbe, D.C. Benner, P.F. Bernath, M. Birk, J. Vander Auwera, J. Quant. Spectrosc. Radiat. Transfer 110 (9) (2009) 533–572. <http://www.cfa.harvard.edu/hitran/>.
[32] S.H. Pyun, J. Cho, D.F. Davidson, R.K. Hanson, Meas. Sci. Technol. 22 (2) (2011) 025303.
[33] Z. Hong, R.D. Cook, D.F. Davidson, R.K. Hanson, J. Phys. Chem. A114 (18) (2010) 5718–5727.
[34] D. Richter, P. Weibring, A. Fried, O. Tadanaga, Y. Nishida, M. Asobe, H. Suzuki, Opt. Express 15 (2) (2007) 564–571.
[35] E.A. Irdam, J.H. Kiefer, Chem. Phys. Lett. 166 (5) (1990) 491–494.
[36] S. Hochgreb, F.L. Dryer, J. Phys. Chem. 96 (1) (1992) 295–297.
[37] H. Wang, X. You, A.V. Joshi, S.G. Davis, A. Laskin, F. Egolfopoulos, C.K. Law, USC Mech Version II, 2007. <http://ignis.usc.edu/USC_Mech_II.htm>.
[38] G. Friedrichs, D.F. Davidson, R.K. Hanson, Int. J. Chem. Kinet. 36 (3) (2004) 157–169.
[39] T. Bentz, F. Striebel, M. Olzmann, J. Phys. Chem. A112 (27) (2008) 6120–6124.